Drug Delivery and Translational Research
https://doi.org/10.1007/s13346-019-00671-w

ORIGINAL ARTICLE

Artificial neural network for modeling formulation and drug permeation of topical patches containing diclofenac sodium

Sonia Lefnaoui[1,2] · Samia Rebouh[1,2] · Mounir Bouhedda[3] · M. Madiha Yahoum[2]

Abstract

In this work, topical matrix patches of diclofenac sodium (DS) were formulated by the solvent casting method using different ratios of chitosan (CTS) and kappa carrageenan (KC). Propylene glycol and tween 80 were used as a plasticizer and permeation enhancer, respectively. The drug matrix film was cast on a polyvinyl alcohol backing membrane. All the patches were evaluated for their physicochemical characteristics (thickness, folding endurance, flatness, drug content, tensile strength, bioadhesion, moisture content, and moisture uptake), along with their in vitro release and in vitro skin permeation studies. Franz diffusion cells were used to conduct the in vitro permeation studies. The artificial neural network (ANN) model was applied to simultaneously predict the DS release and the ex vitro skin permeation kinetics. The formulated patches showed good physicochemical properties. Out of all the studied patches, F6 presented sustained permeation in 32 h and was selected as the best formulation. The ANN model accurately predicted both the kinetic release and the skin permeability of DS from each formulation. This performance was demonstrated by the obtained $R^2 = 0.9994$ and $R^2 = 0.9798$ for release and permeation kinetics modeling, respectively, with root mean square error (RMSE) = 3.46×10^{-5}.

Keywords ANN modeling · Diclofenac sodium · Diffusion · In vitro skin permeation · Topical patches

Introduction

The skin forms the most important frontier of the body that separates the external environment from internal organs. The skin is often chosen as the administration route for drugs when local and systemic therapeutic effects are sought. However, it is challenging and difficult for several drugs to be successfully administered in topical form because the skin prominently protects the body from outside entities. Moreover, drugs designed to be administered transdermally must have potent characteristics that allow them to pass through the stratum corneum and reach the bloodstream in an effective therapeutic dose. Nevertheless, only a few substances have the required characteristics to cross the stratum corneum in sufficient quantities to achieve a therapeutic concentration in the blood [1, 2].

The transdermal route of administration eliminates frequent drug dosing for patients and avoids plasma level peaks. Thus, the plasma concentrations of drugs remain constant, especially during long treatments, such as those of chronic diseases. On the other hand, a drug with a short half-life is the best candidate for transdermal administration [3, 4]. In this context, DS is an active ingredient that has the desired properties for transdermal administration (see Fig. 1). As it is classified as a drug with non-steroidal anti-inflammatory properties (logP = 4.51, pKa = 4.15), it is frequently prescribed for the treatment of

✉ Sonia Lefnaoui
lefnaoui_sonia@yahoo.fr; http://www.univ-medea.dz

Samia Rebouh
samrebouh@yahoo.fr; http://www.univ-medea.dz

Mounir Bouhedda
bouhedda.m@gmail.com; http://www.univ-medea.dz

M. Madiha Yahoum
madihamelha@yahoo.fr; http://www.univ-medea.dz

[1] Laboratory of Biomaterials and Transport Phenomena (LBMPT), University of Medea, Algeria, Nouveau Pôle Urbain, Medea University, 26000 Medea, Algeria

[2] Faculty of Sciences, University of Medea, Algeria, Nouveau Pôle Urbain, Medea University, 26000 Medea, Algeria

[3] Laboratory of Advanced Electronic Systems (LSEA), University of Medea, Algeria, Nouveau Pôle Urbain, Medea University, 26000 Medea, Algeria

Published online: 04 September 2019

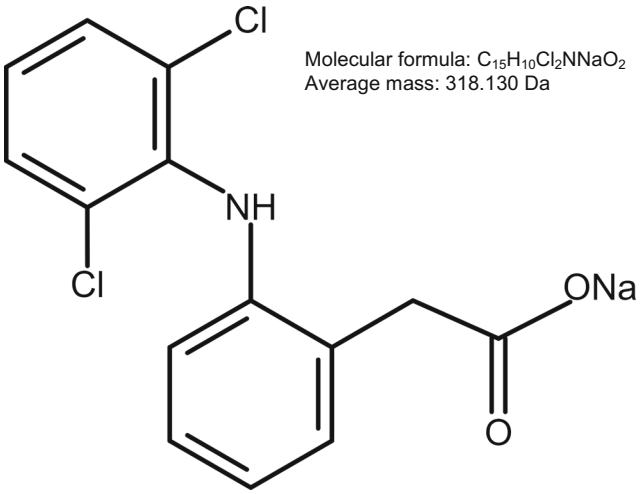

Fig. 1 Chemical structures of diclofenac sodium (DS)

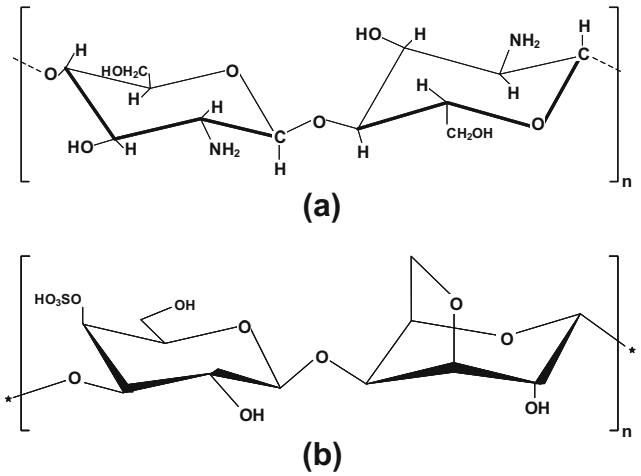

Fig. 2 Chemical structures of (a) Chitosan (CTS) and (b) κ-Carrageenan (KC)

rheumatoid arthritis, applied to reduce inflammation, and as analgesic pain relief [3, 5]. Hence, to maintain a therapeutic drug blood level of DS, multiple doses are required due to its short biological half-life, which ranges from 1 to 2 h.

However, DS causes several side effects during long-term administration, such as gastrointestinal disorders and peptic ulceration [6, 7]. Several studies were conducted to develop transdermal forms of DS and avoid the oral route for prolonged release and eliminate the side effects caused by the oral dosage forms [8–12].

Currently, natural polymers are commonly applied in the development of pharmaceutical transdermal forms. CTS is a natural polymer that is extensively used in cutaneous formulations because it offers interesting physicochemical properties, such as biocompatibility and biodegradability [13]. Also, CTS is a natural macromolecule-forming hydrogel that can be used as matrix systems in drug release. While CTS was often used as a matrix material in transdermal drug delivery, it is interesting to use it in sustained drug release, combining it with oppositely charged polyelectrolytes to form networks of polyelectrolyte complexes (PECs) [14, 15]. These new polymeric networks are not formed by chemical bonds but are based on electrostatic, hydrophobic, non-covalent, and hydrogen bonding forces. Thus, new properties may appear, and these PECs can be explored as new carriers for prolonged drug release [5, 16, 17].

CTS, derived from chitin, is a natural polymer found in crustacean shells. It is a linear glycosaminoglycan (see Fig. 2a), which consists of N-acetyl-D-glucosamine units. It contains cationic groups of glucopyranose units (amino groups) that interact electrostatically with anionic groups of another polymer, like KC sulfate groups (see Fig. 2b), to form a polyelectrolyte complex. This new polymeric network provides the physicochemical properties required to design transdermal drug delivery systems. Furthermore, the hydrogels formed by this polymeric network are biocompatible, more sensitive to environmental variations, and well tolerated. In this study, a polyelectrolyte complex gel is formulated from natural polysaccharides, namely KC with sulfonate groups, as it is used as a polyanion component. Additionally, CTS has amino groups, and it is used as a polycation component. Hence, these two polyelectrolytes can be used to obtain PECs.

Mathematical or empirical models are often used to understand the role of formulation parameters that optimize the skin permeation and the drug transdermal release and diffusion. These mathematical models represent the release of the drug in a biologically realistic membrane, incorporating three-dimensional diffusion and other variations depending on the time and drug formulations. However, these models are complex and unable to predict the different transport phenomena involved in drug delivery from transdermal patches. On the other hand, intelligent methods are considerably more powerful and were proven to be effective in modeling very complex situations [18, 19]. Research has exploited several intelligent artificial techniques to model many systems by using input-output data sets. ANNs are nonlinear systems inspired by biological neural systems and have proven their reliability and flexibility in several areas, including pharmaceutical technology [20]. An ANN model was employed by Takayama et al. to predict the controlled release of theophylline from tablets based on a hydroxypropyl methylcellulose, lactose, and cornstarch mixture [21]. Many formulations were optimized using the ANN model, for example, nimodipine floating tablet formulation [22], transdermal ketoprofen hydrogel [23], and aspirin extended release tablets [24, 25]. Chen et al. used an ANN and pharmacokinetic simulations to design a controlled release tablet for sympathomimetic drug formulations [26]. The sustained release of DS from matrix tablets was predicted using an ANN model by Zupancic Bozic

et al. [27]. Hussain et al. used ANNs to optimize the controlled release of ketoprofen hydrogel ointment and capsules [28]. In the last few years, we have opted toward the application of intelligent systems based on neural networks to model several drug delivery systems. In one of our recent studies, we operated an adaptive model neuro-fuzzy inference system (ANFIS) to model the release profile of ibuprofen from a matrix tablet based on biopolymers [19]. The ANFIS was a good prediction model in terms of accuracy and robustness for only one input [19, 29]. However, for other studied systems with more than one output, the ANN was a good candidate [18, 30]. In this new study, an interesting approach was adapted that consisted of developing a single intelligent model based on ANNs to predict the two kinetics and the release and diffusion of the DS over time, in order to understand the effect of the formulation parameters on the membrane barrier.

Compared with the traditional mathematical models, less time is required in the implementation of ANNs, the mathematical description of phenomena is not required, and some experiments are sufficient for model development. The ANNs and many other intelligent techniques were exploited using the input-output data sets to model complex systems. The application of ANN in DS delivery from stamps or membrane was not previously studied; only a single study has focused on the prediction and optimization of estradiol release of ethylene-vinyl acetate membranes by ANN [31].

The present research focuses on the development of a transdermal drug delivery system for diclofenac and the optimization of an ANN structure that can predict its biopharmaceutical profile. Our study will allow us to obtain a comparative efficacy of such delivery systems in terms of the increase in drug transport and sustained drug release from polyelectrolyte support based on biopolymers. Furthermore, the ANN modeling can predict the impact of the patch formulation parameters on both the diclofenac permeation and diffusion kinetics without resorting to experience. This gives our intelligent system two benefits, precision and robustness, compared with the many mathematical models, which are sometimes inadequate, and economical and practical values where we do not need to perform all the experiments to see the results.

In this current work, the development of topical patches of DS, formulated with CTS and KC with different ratios, was conducted. The main objective was to optimize the in vitro release of drugs and permeation properties to obtain sustained release from topical patches. Also, an optimum combination of CTS and KC polymers was identified to obtain an effective drug level for an extended period. Furthermore, an ANN was developed to model and predict the kinetic profile of release and diffusion of the DS from the developed transdermal membranes.

Materials and methods

Materials

The active ingredient, DS, was donated by Antibiotical Laboratories (Saidal Industries, Algeria). Tween 80 (T_{80}) was supplied by BDH (UK). Polyvinyl alcohol (PVA) was supplied by Sigma-Aldrich (UK). Propylene glycol (PG) was purchased from Merck (Germany). CTS with a molecular weight (*M*w) of 210,000 g mol^{-1} was purchased from Sigma-Aldrich (USA). KC with an *M*w of 285,000 g mol^{-1} was obtained graciously from Orkila (Algeria). All other chemicals were purchased from Merck (Germany).

Preparation of topical patches

The formulation of DS-loaded topical patches was performed by the solvent casting method with different ratios of CTS and KC, as indicated in Table 1. The first step consisted of the preparation of the backing membrane by pouring 10 ml of a PVA solution (3%, w/v) in a Petri dish. The obtained film was left to dry in ambient air for 24 h. Subsequently, solutions of CTS and KC (1.0%, w/w) with PG (2.0%, v/w) as plasticizer were prepared separately in an aqueous solution (1%, v/v) of acetic acid and distilled water, respectively. The resulting solutions were then filtered and stored for 24 h until it was needed. Both solutions were mixed at different proportions and vigorously stirred at 75 °C with magnetic agitation until the mixture reached room temperature. Later on, T_{80} (1.0%, v/w) was added as a permeation enhancer. The loading of the drug (1.3%, w/w) was carried out by homogeneous dispersion, with slight mechanical stirring, to obtain matrix patches containing 6 mg/cm^2 of DS. The dispersion was poured onto the backing membrane and dried at 40 °C for 12 h. Finally, a gummy tape was then adhered to the support membrane keeping the matrix side up. The drug matrices were kept in desiccators until their characterization.

Evaluation of topical patches

Study of compatibility between the drug and polymers

A Fourier Transform IR spectrometer, FTIR (Perkin-Elmer, USA), was used to investigate the probable interaction between the DS and the polymers of the patches by using the KBr pellet method. These pellets were scanned via wavelengths ranging from 4000 to 400 cm^{-1}. The analysis was performed on pure DS and physical mixtures of DS with CTS and KC [32]. Also, a comparative spectral study was conducted using Opus software (version 7.5, build: 7, 5, 18), wherein the presence of the main bands in DS and the physical mixtures were assessed.

Table 1 Formulation variables of diclofenac topical patches

Formulation number	Ratio CTS:KC	Total weight of polymer (mg)	CTS weight (mg)	KC weight (mg)
F1	10:0	400	400	0
F2	9:1	400	360	40
F3	8:2	400	320	80
F4	7:3	400	280	120
F5	6:4	400	240	160
F6	5:5	400	200	200
F7	4:6	400	160	240
F8	3:7	400	120	280
F9	2:8	400	80	320
F10	1:9	400	40	360
F11	0:10	400	0	400

Uniformity of thickness and appearance

The thickness and the morphological appearance of all the prepared patches were examined [32, 33]. For each formulation, three random patches were selected, and their mean values were determined. The thickness of these patches was assessed at five different points on each patch (digital caliper, Mitutoyo Co., Japan).

Folding endurance

The folding endurance (FE) capacity refers to the resistance of the patches that are subjected to frequent extreme folding conditions and depicts the brittleness of the patches. FE is assessed by constantly folding the films (2 cm × 2 cm) at the same place until they break. The FE value is the number of times these films can be folded in the same place without breaking [32, 33].

Flatness

A flatness study indicates that a topical patch does not constrict with time and has a smooth surface. The patches were cut into long strips, and the length of every strip was measured to determine the flatness of the patches. The length variation was calculated by the constriction percentage, using Eq. (1), in which a 0% constriction was equal to a 100% flatness [32, 33].

$$\text{Constriction}\ (\%) = \frac{I_1 - I_2}{I_1} \times 100 \quad (1)$$

where I_2 is the final length of every single strip and I_1 is the initial length of each strip.

Drug content

The drug content of the DS formulations was analyzed in triplicate via a high-performance liquid chromatography (HPLC) [34]. For this purpose, a C_{18} column (250 mm × 4.6 mm × 5 μm) was used to separate the samples in an oven with a temperature of 45 °C; samples of 20 μl were injected into the column, and the resulting peaks were monitored at 284 nm. The mobile phase (0.2% triethylamine and acetonitrile (40:60% v/v) with pH 2.75 that was adjusted using 85% phosphoric acid) was maintained in an isocratic mode at a flow rate of 1 ml/min. The used HPLC instrument (Perkin-Elmer, USA) is composed of a pump, auto-sampler, and online vacuum degasser, and a Peltier column oven linked by a PE Nelson Network Chromatography Interface (NCI) 900 with a UV/VIS (series 200). Perkin-Elmer TotalChrom Workstation Software (version 6.3.1) was used for the HPLC analysis.

Moisture content study

All the patches were individually weighed and stored in a desiccator with calcium chloride salt for 24 h at room temperature. Subsequently, these patches were reweighed after a specific time interval until a constant weight was achieved. The percentage of the moisture content (MC) was estimated after calculating the difference between the initial and final weights using Eq. (2) [32, 33]:

$$\text{Moisture content}\ (\%) = \frac{\text{Initial weight–Final weight}}{\text{Final weight}} \times 100 \quad (2)$$

Moisture uptake

A saturated potassium chloride solution was placed in the desiccator to maintain a relative humidity of 84%. The weighed films were kept in the desiccator at room temperature. After 24 h, these films were reweighed, and the percent moisture uptake (MU) was calculated using Eq. (3) [32, 33]:

$$\text{Moisture uptake}\ (\%) = \frac{\text{Final weight–Initial weight}}{\text{Initial weight}} \times 100 \quad (3)$$

Evaluation of mechanical properties

Pharmaceutical patches should exhibit good mechanical properties to maintain their integrity while handling. The influence of the polymer ratio was evaluated to improve the mechanical properties of all the formulations. A high tensile strength value indicates that the patches have good mechanical strength. Strips of topical films (2×2 cm^2) were statically placed between the jaws (distance between jaws is 2 cm) of the tensile testing machine (ZwickRoell, Germany), at a tensile speed of 10 mm/min to determine the tensile strength values. The study was carried out three times for each formulation. The measurements were conducted until the film broke [35].

Bioadhesion properties

The bioadhesive strength of all the formulations was measured using a technique described earlier by Gupta et al. with a few modifications [36]. The excised rat abdominal skin (Wistar albino) was statically placed on the open mouth of a glass vial that was filled with phosphate buffer, pH 7.4. This glass vial was placed firmly in a beaker that was filled with the same buffer and was incubated at 37 ± 0.5 °C. These patches were glued to the lower side of the rubber stopper. The mass (g) needed to detach these patches from the skin surface showed the bioadhesive strength (BS) of the patches (see Fig. 3). The force of adhesion (N) was estimated from the BS measurements using Eq. (4) [37]:

$$\text{Force of adhesion}\ (N) = \frac{\text{Biaodhesive strength} \times 9.81}{1000} \quad (4)$$

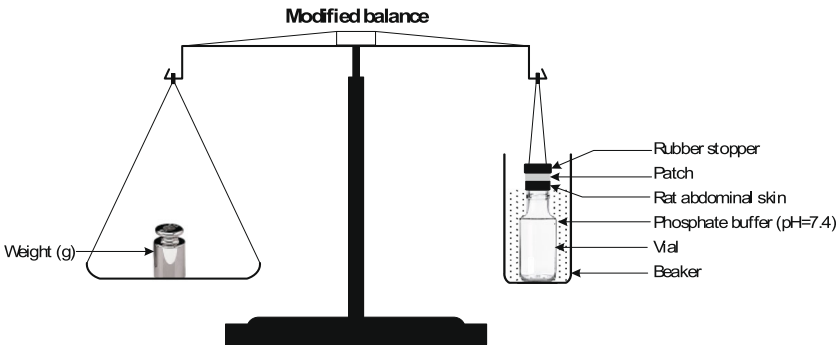

Fig. 3 Bioadhesion test assembly (modified balance)

In vitro dissolution kinetics

The dissolution kinetics study was conducted in a USP dissolution device (SotaxAT7 smart dissolution testing unit, Germany) that contains six rotating cylinders. These glass containers were filled with 900 ml of phosphate buffer (pH 7.4), kept at 32 ± 0.5 °C, and stirred at 50 rpm. The patches were placed against a watch glass and kept fixed using mesh and stainless steel clips centered at the bottom of the vessels with their release surfaces facing upwards [38]. During the test, 5-ml samples were regularly collected at every 2-h interval for 32 h. An equal volume of the phosphate buffer (pH 7.4) was added to the cylinders to replace the regularly removed volume. The amount of drug released was determined by the HPLC method [34]. The results of the drug release kinetics were fitted to the zero-order equation (Eq. (5)) and the Korsmeyer–Peppas equation (Eq. (6)) [39]:

$$M_t = M_0 + k_0 t \quad (5)$$

$$\frac{M_t}{M_\infty} = kt^n \quad (6)$$

where M_t refers to the amount of drug released in time t, M_0 denotes the amount of drug in a dosage form, M_∞ is the amount of drug released in infinite time, k_0 and k refer to the release rate constants, t is the time, and n is the release exponent. The n value indicates the mechanism that can control the drug release. If n is close to 0.5, a Fickian or diffusion-controlled release is involved, whereas when $0.5 < n < 1.0$, a non-Fickian transport occurs, and when $n = 1$, the zero order is involved; for $n > 1$, a super case II transport is confirmed.

In vitro skin permeation

The evaluation of the in vitro skin permeation was performed using Franz diffusion cells (SES Franz Cells, Analyze System,

GmbH Germany). These permeation tests were conducted on excised rat abdominal skin (Wistar albino) that was placed between the donor and the receiver compartments (60 ml) of the diffusion cell. After the patches were placed on the rat skin, they were coated with parafilm. The receptor compartment was filled with phosphate buffer (pH = 7.4) and magnetically stirred at 50 rpm at 32 ± 0.5 °C [32, 40]. Regular samples were taken from this compartment, and the amount of drug that diffused through the skin was assessed using the HPLC analysis. After each sample, an identical volume of the medium was replaced with fresh phosphate buffer (pH 7.4).

The results of the cumulative amount of the drug that permeated per unit area (Q, mg/cm^2) versus time (t, h) were plotted. After that, the flux (J, mg cm^{-2} h^{-1}) was determined as the slope of the linear region of the graph. The x-intercept of the curve at steady state represents the lag time (Lgt, h).

The steady state permeability coefficient (Kp, cm h^{-1}) was estimated using Eq. (7):

$K_p = J/C_D$ (7)where C_D represents the concentration of the drug in a donor compartment.

ANN modeling of the release and diffusion of diclofenac

An ANN was developed to predict the kinetic profile of the in vitro release and the in vitro permeation of the DS from the prepared transdermal membranes. There were originally three inputs of the system, time, CTS amount, and KC amount, in the formulations. Two outputs were determined, the cumulative drug release and the cumulative drug permeation per unit area over time.

ANN basics

The search for optimized operating conditions is done through the modeling of the studied process. One of the main problems regarding drug release is the difficulty in obtaining a model that represents the kinetic release profile and rate according to the formulation parameters. A neural network could be considered as an intelligent system composed of several units of nonlinear computation (neurons) that operate in parallel and are connected by weights. Neural networks with satisfactory results could model many processes for implementing optimal driving strategies.

The implementation of neural networks consists of two phases: a learning phase and a validation phase. The problem of learning in a neural network, an input-output function from a set of experimental data, is equivalent to the problem of synthesis of associative memory that finds the appropriate output for a presented input and proceeds to a generalization when it comes to new input. In other words, a neural network can be associated with a nonlinear (rather complex) function that connects the outputs to the inputs. The learning phase is only the identification of the parameters of this function (network weights) such that the outputs calculated by the network are as close as possible to those observed (target values). In general, learning is performed over a relatively long period and consists of four calculation steps:

1. Choose an adequate architecture, as illustrated in Fig. 4.
2. Initialize the network weights.
3. Presentation and propagation of the input vector to the network output layer (calculation of the outputs by the network) (see Fig. 5).
4. Calculation of error between calculated and observed outputs.
5. Calculation of the correction vector. Corrections are determined from the values of the error to update the values of the connection weights between the neurons.

Three databases were used for network development and validation, a learning base, a test base that serves to learn the network, and the validation base. The first one is used to find an optimized weight set, and the second one is used to validate optimized weights and avoid overtraining. The last base is used to run the neural network and test its generalization capacity. The Levenberg-Marquardt (LM) algorithm was adopted for the learning phase; it was supervised learning. This algorithm used the learning database to update the weights iteratively using Eqs. (8) and (9) by minimizing the mean square error given in Eq. (10).

$$w_{ij}(k) = w_{ij}(k-1) - \left[\mathbf{J}^T\mathbf{J} + \mu\mathbf{I}\right]^{-1}\mathbf{J}^T\varepsilon_i(k-1) \quad (8)$$

$$b_i(k) = b_i(k-1) - \left[\mathbf{J}^T\mathbf{J} + \mu\mathbf{I}\right]^{-1}\mathbf{J}^T\varepsilon_i(k-1) \quad (9)$$

$$MSE = \frac{1}{M}\sum_{k=1}^{M}\sum_{i=1}^{L}\left(y_i^k - z_i^k\right)^2 \quad (10)$$

The output error corresponding to the i^{th} node is ε_i ; $\mathbf{J}$ is the Jacobian matrix that involves the first derivatives of the network errors with respect to the weights; μ is the learning coefficient; k corresponds to the index iteration of the learning algorithm; M is the number of iterations of the LM algorithm; L is the number of outputs; and y_i is the i^{th} ANN desired output.

Model validation

Validation helps determine the model's ability to replicate the same behavior. Two different criteria were selected: the correlation coefficient (R^2) and a RMSE, shown in Eqs. (11) and (12), respectively.

Fig. 4 Architecture of ANN

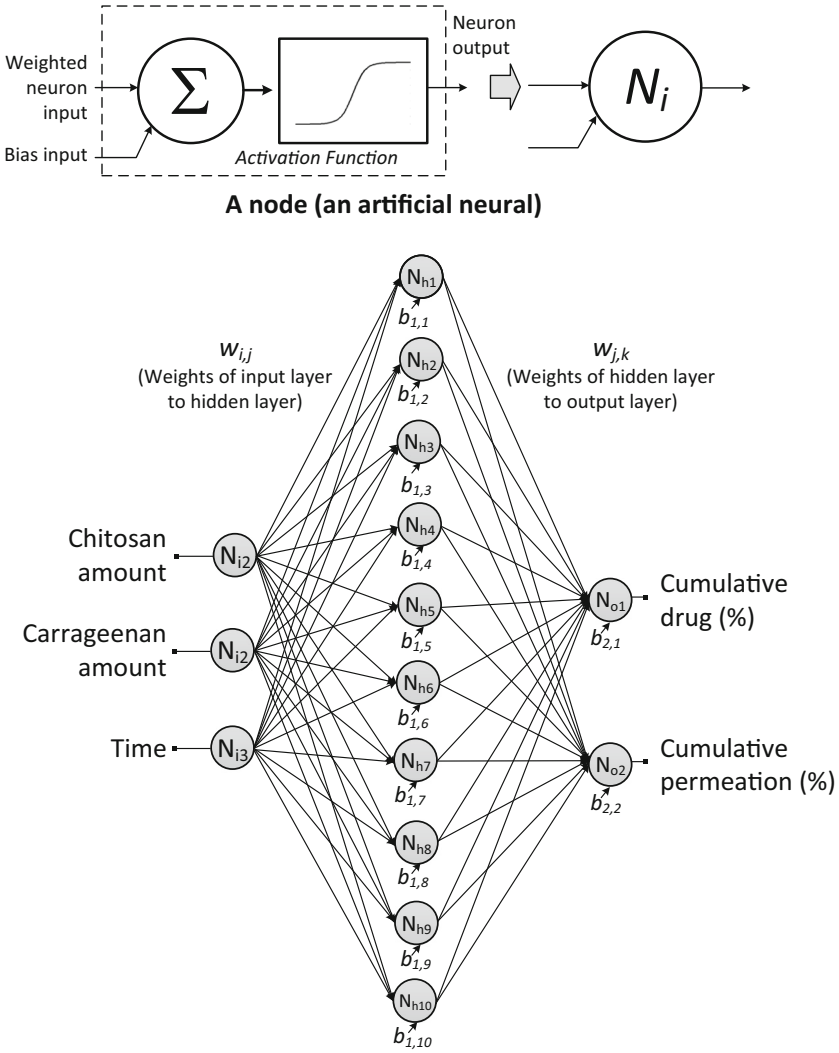

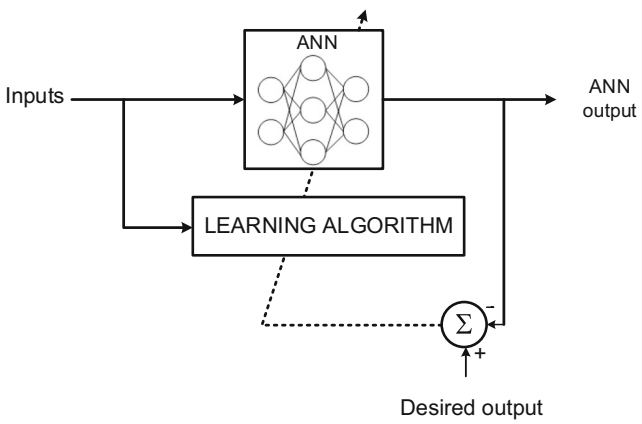

Fig. 5 ANN supervised learning

$$R^2 = \frac{1}{N}\frac{\sum_{i=1}^{N}\left(y_s-\overline{y}_s\right)\left(y_e-\overline{y}_e\right)}{\sigma_s\sigma_e} \tag{11}$$

$$RMSE = \sqrt{\frac{\sum_{i=1}^{N}\left(y_s-y_e\right)^2}{N}} \tag{12}$$

For the same input conditions, y_s is the ANN predicted output value and y_e is the experimental value; N is the number of samples and σ_s and σ_e are the standard deviations (SD) of the distributions y_s and y_e.

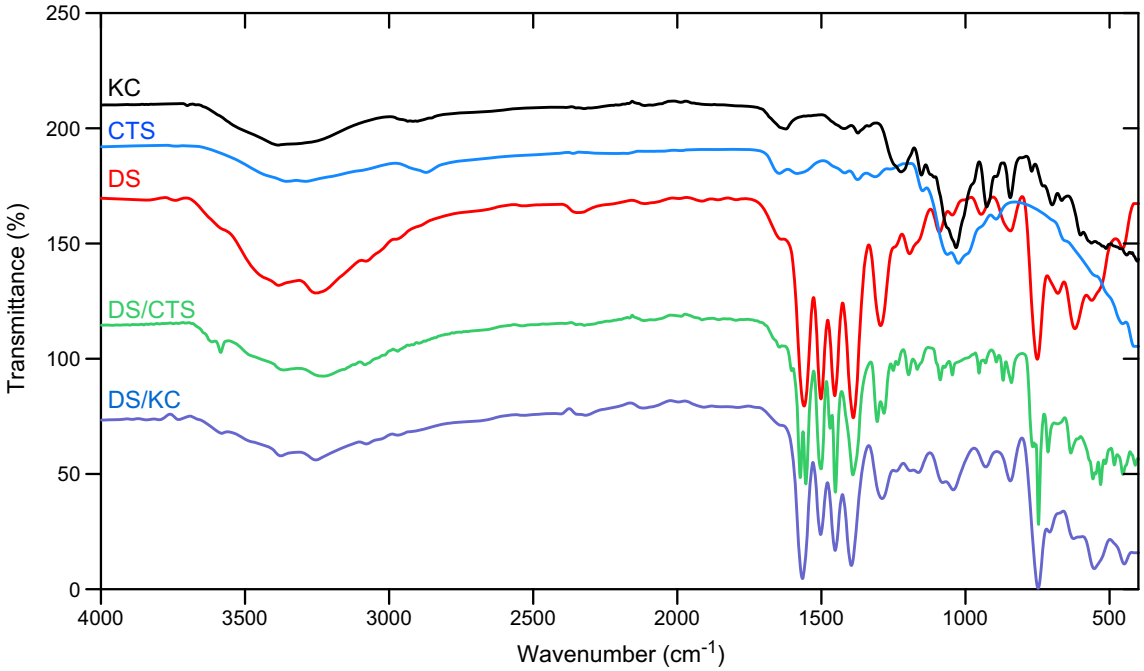

Fig. 6 FTIR spectra of diclofenac sodium (DS), chitosan (CTS), kappa carraggenen (KC), physical mixture of diclofenac sodium kappa carraggenen (DS/KC), and physical mixture of diclofenac sodium and chitosan (DS/CTS)

Results and discussions

Drug-polymers interaction studies

The FTIR spectra of pure DS and physical mixtures of DS with KC and CTS are illustrated in Fig. 6. The DS spectrum showed stretching vibration bands at 1690 cm^{-1} that corresponded to C=O groups. A broad absorption in the range of 3100–2400 cm^{-1} indicates aliphatic –CH region bonds. The bands at 1510 cm^{-1} and 1400 cm^{-1} were assigned to –NH and aliphatic (–CH2, –CH3) groups respectively. A characteristic band at 1570 cm^{-1} was attributed to the C=C vibration. The bands at 3450 cm^{-1} and 3265 cm^{-1} were associated with the –NH vibrations and the bands at 2150 cm^{-1} and 1620 cm^{-1} were assigned to the aromatic groups. Furthermore, the vibration around 1690 cm^{-1} indicated the presence of the carboxyl group –COOH, and the band at 745 cm^{-1} corresponded to the CCl vibrations [41]. The main bands in the DS spectrum were also displayed in the DS physical mixtures with the CTS and KC biopolymers, which indicated the absence of interactions between these excipients and the DS [41, 42].

Table 2 Physicochemical properties of DS topical patches

Form no.	Ratio CTS:KC	Physicochemical properties					Bioadhesion properties	Mechanical properties
		Thickness (mm)	FE (%)	MC (%)	MU (%)	Drug content (%)	Force of adhesion (N)	Tensile strength (Kg/cm^2)
F1	10:0	1.25 ± 0.02	260 ± 3.54	3.24 ± 0.04	6.25 ± 0.03	99.12 ± 0.52	0.35 ± 0.02	1.08 ± 0.02
F2	9:1	1.22 ± 0.04	254 ± 4.25	3.62 ± 0.01	6.85 ± 0.02	99.25 ± 0.42	0.38 ± 0.03	1.15 ± 0.05
F3	8:2	1.23 ± 0.02	248 ± 6.85	3.74 ± 0.11	7.22 ± 0.05	99.54 ± 0.21	0.40 ± 0.02	1.28 ± 0.04
F4	7:3	1.24 ± 0.04	242 ± 4.12	3.86 ± 0.06	7.65 ± 0.11	99.53 ± 0.35	0.41 ± 0.01	1.31 ± 0.01
F5	6:4	1.22 ± 0.05	240 ± 3.15	4.22 ± 0.04	8.22 ± 0.13	98.98 ± 0.24	0.43 ± 0.02	1.38 ± 0.04
F6	5:5	1.25 ± 0.01	238 ± 2.84	4.85 ± 0.02	8.65 ± 0.12	99.98 ± 0.28	0.45 ± 0.03	1.42 ± 0.01
F7	4:6	1.24 ± 0.05	229 ± 5.57	4.52 ± 0.02	9.12 ± 0.11	99.56 ± 0.14	0.41 ± 0.02	1.25 ± 0.05
F8	3:7	1.25 ± 0.03	220 ± 2.12	4.27 ± 0.09	9.22 ± 0.05	99.46 ± 0.12	0.38 ± 0.02	1.18 ± 0.02
F9	2:8	1.23 ± 0.02	218 ± 3.01	3.65 ± 0.02	9.35 ± 0.04	99.54 ± 0.25	0.35 ± 0.01	1.11 ± 0.03
F10	1:9	1.24 ± 0.03	210 ± 4.63	3.32 ± 0.01	9.44 ± 0.18	99.35 ± 0.32	0.32 ± 0.03	0.85 ± 0.04
F11	0:10	1.22 ± 0.01	208 ± 4.25	3.12 ± 0.02	9.52 ± 0.15	99.65 ± 0.41	0.30 ± 0.01	0.65 ± 0.09

The results are expressed as the mean ± standard deviation ($n = 3$)

Physicochemical characterization of patches

The set of patches formulated by the solvent casting technique were subjected to specific tests to evaluate their physicochemical characteristics, and the results must conform to the requirements of topical patches [43]. The results are summarized in Table 2 and expressed as mean ± standard deviation ($n = 3$). Statistical analysis of the study was conducted by ANOVA using Tukey's one-way method with Sigma-Plot 11.0 software. A p value less than or equal to 0.05 was considered to be statistically significant. The film thickness ranged between 1.22 ± 0.01 and 1.25 ± 0.02 mm with low standard deviation values, which indicated the uniformity of all the prepared patches. The drug content in the formulated patches varied from 98.98 ± 0.24 to 99.98 ± 0.28%, which confirmed the good dispersion of the DS when the films were formulated. The endurance test (FE) was performed to examine the ability of the patches to maintain proper integrity when applied to the skin. The FE results were properly and accurately exhibited for all the films, and these values increased when the CTS concentration increased in the formulas ($p < 0.05$). The presence of PG (as a plasticizer) enhanced the FE results of the CTS-based films [44]. Plasticizer interferes with chitosan chains by decreasing intermolecular forces, thereby softening the brittleness of the film structure and increasing the polymer mobility, which facilitates the film folding [45, 46]. However, the presence of KC reduced the FE values because the network formation of PECs was based on electrostatic and hydrogen bonding forces between CTS and KC despite the presence of the plasticizer. All the prepared formulations showed 100% flatness with a negligible constriction, illustrating that the patches prepared by the solvent evaporation technique are reproducible, and they can maintain satisfactory surface smoothness.

The tensile strength test (TS) must be validated on all the prepared patches to prove that no crack or breakage is likely to occur while they are in use. For this purpose, the TS test showed no cracks in the films up to values ranging from 0.65 ± 0.09 to 1.42 ± 0.01 kg/cm^2. The TS value increased significantly ($p < 0.05$) when the CTS/KC ratio equals to unity (1:1). The molecular interactions between CTS and KC at the unit ratio led to the formation of the intermolecular bond. This created a stronger gel network where the polysaccharide molecules are closer, forming a more coherent film structure [47]. When a strong intermolecular bonding between the molecules was formed, the film exhibited strong affinity and high tensile strength [48]. Furthermore, the addition of PG as a plasticizer contributed significantly to improving the TS of the patches.

The stability of the patches depends on the low MC values to preserve the patches during storage. Besides, low MC means the patches do not turn brittle while in use. The MC values of the formulated patches were moderate and low; they ranged from 3.12 ± 0.02 to 4.85 ± 0.02%. In the same context, the MU of the studied patches ranged from 6.25 ± 0.03 to 9.52 ± 0.15%, which indicates good protection against microbial contamination. The bioadhesion properties of the patches were evaluated by the force of adhesion (FA) of each formula. The test examined the compatibility of films based on the biopolymers matrices with the skin when the patches were applied. The obtained values showed an excellent adhesion force, varying from 0.30 ± 0.01 to 0.45 ± 0.03 N, indicating a statistically significant increase of FA ($p < 0.05$) when the CTS/KC ratio is of the order of one.

Drug release kinetics

The in vitro dissolution test was performed to monitor the drug release from the formulated patches, the cumulative drug release as a function of time variation (see Fig. 7), and to determine $t_{10\%}$, $t_{50\%}$, and $t_{90\%}$ that correspond to the times of the drug's release of 10%, 50%, and 90%, respectively (see Fig. 8). It was observed that all the formulations released the total amount of the loaded drug over 30 h. The dissolution profiles varied with the composition of the polymeric matrix. Thus, the fastest release was observed in formula F1, where 50% and 90% drug release were observed for 10.52 ± 0.41 h and 21.17 ± 0.52 h, respectively. In contrast, a drug release of 99.51 ± 0.65% over 32 h was noted in the F6 formulation, with 50% and 90% of the loaded drug released in 4.40 ± 0.52 h and 16.84 ± 0.47 h, respectively. The results demonstrate the important role of the CTS/KC polymer ratios on the dissolution profile. Formulations containing a high proportion of CTS (F1 and F2) showed a faster release of the drug, in less than 24 h only, compared with other formulations (F3–F11). However, when the CTS/KC ratio is in the range of 1/1, total drug release was reached after 32 h. Thus, the DS release was significantly retarded in the F6 patch formulated with a CTS/KC ratio of 1/1, with release times of 10%, 50%, and 90% of 4.40 ± 0.11 h, 16.84 ± 0.14 h, and 27.48 ± 0.62 h respectively. The formation of the CTS/KC polyelectrolyte complex allowed the sustained release of the drug [49, 50]. It should be noted that the complexation of polyelectrolytes between oppositely charged biopolymers results in the formation of polymeric network supports with the potential to modulate the initial burst release as well as the sustained release of drugs [51]. This effect can be attributed to the new structures that emerged from these polymers after the formation of the PEC [52].

In the DS dissolution study, the CTS with many amino groups in its structure was easily protonated and formed a PEC with the anionic KC groups to retard the release of the drug. Thus, the formation of the hydrogel-shaped PEC should slow down the flow of the drug out of the patches, which eventually delayed its release [53]. The influence of CTS in combination with KC on the release of DS from the patches increased when the ratio between the two biopolymers is close to unity. Furthermore, the prolonged release of the drug was also due to the slow dissolution of the PEC in the phosphate-buffered saline medium, which caused the decrease of the solvent penetration rate due to the formation of a more resistant CTS-KC hydrogel on the surface of the patch with a slower dissolution rate [33, 35].

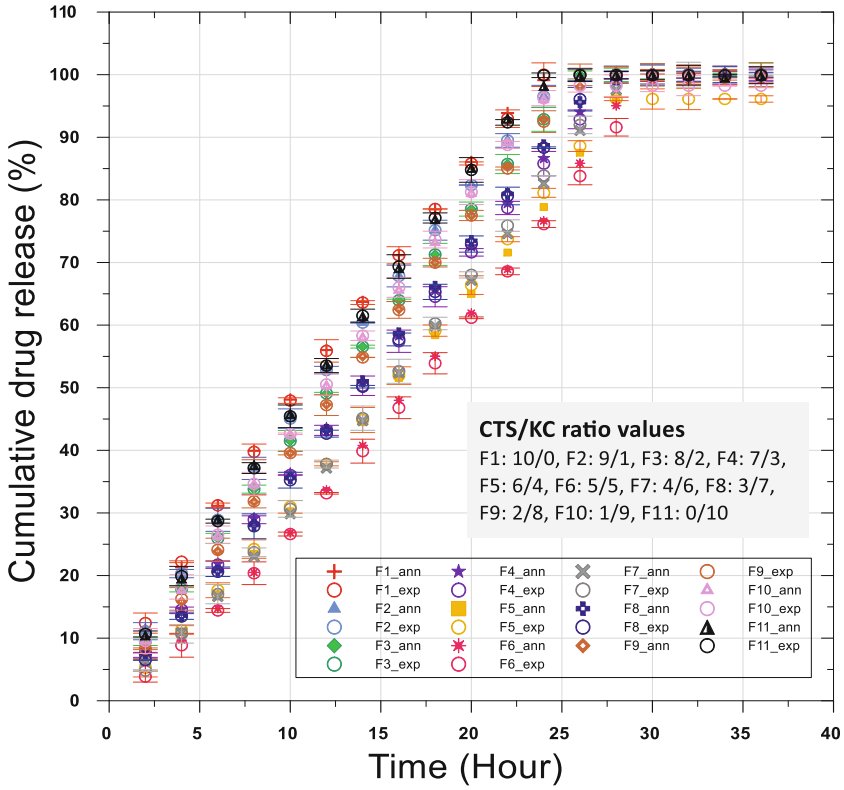

Fig. 7 Experimental and predicted cumulative DS release from topical patches

Nevertheless, the PECs formation was governed by the charge density of the CTS and KC biopolymer molecules; however, the formed complex was dependent on the conformation (coil–helix) of KC molecules in the solutions [54, 55]. Also, no burst release was observed in the formulations studied, with release times of 10% DS ranging from 1.55 ± 0.12 to 4.40 ± 0.11 h. Given the

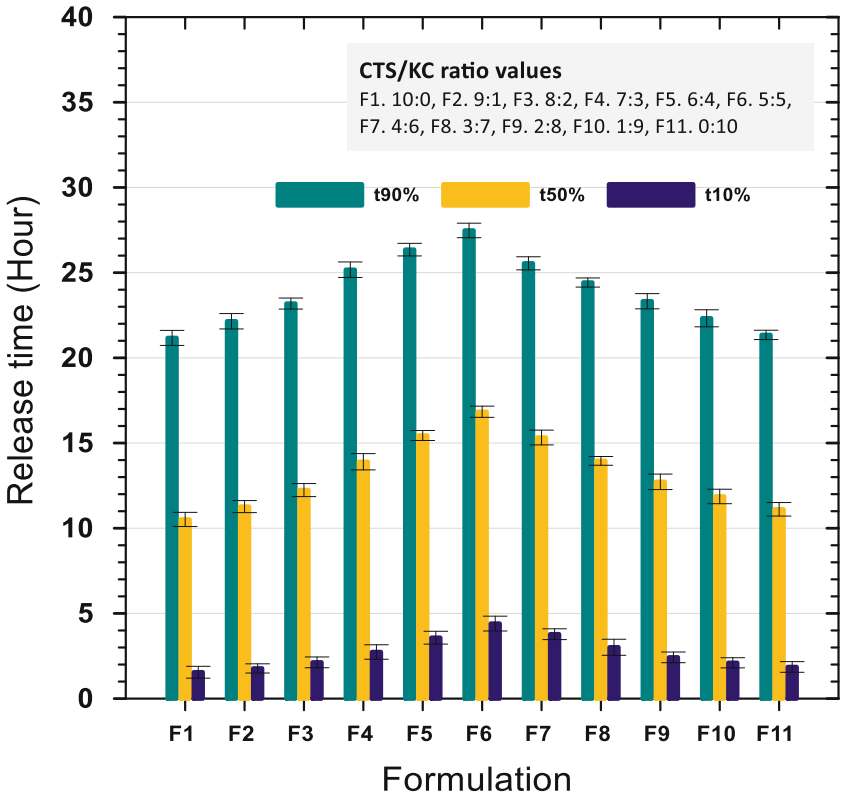

Fig. 8 Release times of 10%, 50%, and 90% of DS from topical patches

Table 3 Model fitting results of in vitro release of DS from transdermal formulations

No.	Ratio CTS:KC	Korsmeyer–Peppas			Zero-order		Release mechanism
		k^a	n^a	R^2	$k_0{}^a$	R^2	
F1	10:0	6.93 ± 0.03	0.84 ± 0.01	0.998	4.37 ± 0.09	0.982	Anomalous transport
F2	9:1	6.08 ± 0.05	0.87 ± 0.04	0.999	4.11 ± 0.015	0.984	Anomalous transport
F3	8:2	4.99 ± 0.08	0.92 ± 0.03	0.998	3.94 ± 0.08	0.996	Anomalous transport
F4	7:3	3.69 ± 0.02	0.99 ± 0.01	0.997	3.58 ± 0.14	0.998	Anomalous transport
F5	6:4	2.46 ± 0.05	1.1 ± 0.02	0.998	3.33 ± 0.13	0.996	Anomalous transport
F6	5:5	1.69 ± 0.04	1.2 ± 0.01	0.999	3.13 ± 0.08	0.986	Anomalous transport
F7	4:6	2.17 ± 0.06	1.15 ± 0.04	0.999	3.42 ± 0.16	0.992	Anomalous transport
F8	3:7	3.14 ± 0.02	1.05 ± 0.03	0.998	3.63 ± 0.14	0.998	Anomalous transport
F9	2:8	4.24 ± 0.04	0.97 ± 005	0.998	3.88 ± 0.11	0.998	Anomalous transport
F10	1:9	5.01 ± 0.06	0.93 ± 0.04	0.998	4.03 ± 0.08	0.992	Anomalous transport
F11	0:10	5.73 ± 0.07	0.90 ± 0.03	0.995	4.29 ± 0.09	0.994	Anomalous transport

[a] Each value represents the mean ± standard deviation ($n = 6$)

experiment results, it was shown that the combination of cationic CTS and anionic KC polymers made it possible to obtain sustained-release support for the delivery of DS [56]. Release of the drug was maintained by polyelectrolytes complexation between oppositely charged polymers, which resulted in the formation of polymeric carriers that had the potential to modulate the initial burst as well as the sustained release of drug-loaded patches [49, 52].

The mechanism of drug release from transdermal patches was confirmed by fitting the experimental results to various kinetic models, such as zero-order and Korsmeyer–Peppas equations, to understand the order and mechanism of DS release. The results are summarized in Table 3, where the coefficients of determination (R^2) are computed for every model. The highest R^2 values of all studied topical patches were found when in vitro dissolution data was fitted to the Korsmeyer–Peppas equation, which indicated the better-fit model to express the in vitro release behavior of DS. The release exponent values (n) calculated from the Korsmeyer–Peppas model (Table 3) indicated that when the n value was higher, the release rate was lower, as the diffusion was partially governed by swelling when the values of n were high [57, 58]. According to the obtained results, the release of the drug from the topical patches system was an anomalous transport mechanism ($0.5 < n < 1$). Therefore, all the results demonstrated a non-Fickian diffusion, indicating a combination of drug diffusion and matrix erosion that controlled the rate release of the drug [16, 59].

In vitro skin permeation studies

Even though rat skin showed higher permeation rates compared with human skin, the permeation kinetic parameters of rat skin are frequently comparable with human skin [60, 61]. However, a fairly good relationship was observed in drug permeation between human skin and hairless rat skin when in vitro skin permeation experiments were conducted in appropriate conditions [62]. Differences in skin permeation kinetics on the effects of certain enhancers on rat and human skin have been observed. Regarding rat skin, comparable kinetics parameters with human skin are observed and could be used for the calculation of skin permeation parameters such as flux, permeability coefficient, partition coefficient, and diffusion coefficient of topically applied drugs [62, 63].

The in vitro dermal permeation study of DS from topical patches across the abdominal skin of an albino rat is illustrated in Fig. 9. The results of the permeation kinetics of the drug per unit area over time showed that the patches released the loaded drug over a prolonged period of 36 h. The curves of the cumulative drug permeation per unit area over time showed straight lines for all formulations, which revealed that the drug permeation from the patches followed zero-order release kinetics.

As presented in Fig. 10, the permeation rates of the drug ranged from 0.168 ± 0.008 to 0.185 ± 0.007 mg cm^{-2} h^{-1}. These results were improved because tween 80 was used as a penetration enhancer across the barrier of the stratum corneum. The permeability coefficients (Kp) ranged from 0.0225 ± 0.005 to 0.0247 ± 0.003 cm h^{-1}. The lag time (Lt) decreased when the proportion of CTS or KC increased in all prepared formulations, and the Lt values ranged from 0.04 ± 0.002 to 0.40 ± 0.001 h. According to these results, the formation of PECs between the CTS and the KC created compact and ordered structures [15]. Thus, the PECs were able to sustain the permeation of the drug [52, 64]. Certainly, a CTS/KC polyelectrolyte complex hydrogel formed a barrier and slowed the flow permeation of the drug. The influence of CTS in combination with KC on the release of DS from the patches was observed when the CTS/KC ratio was 1:1. The calculated permeation data indicated that formation of the complex between CTS and KC controlled and sustained the drug permeation by forming a CTS/KC polyelectrolyte complex [14, 65].

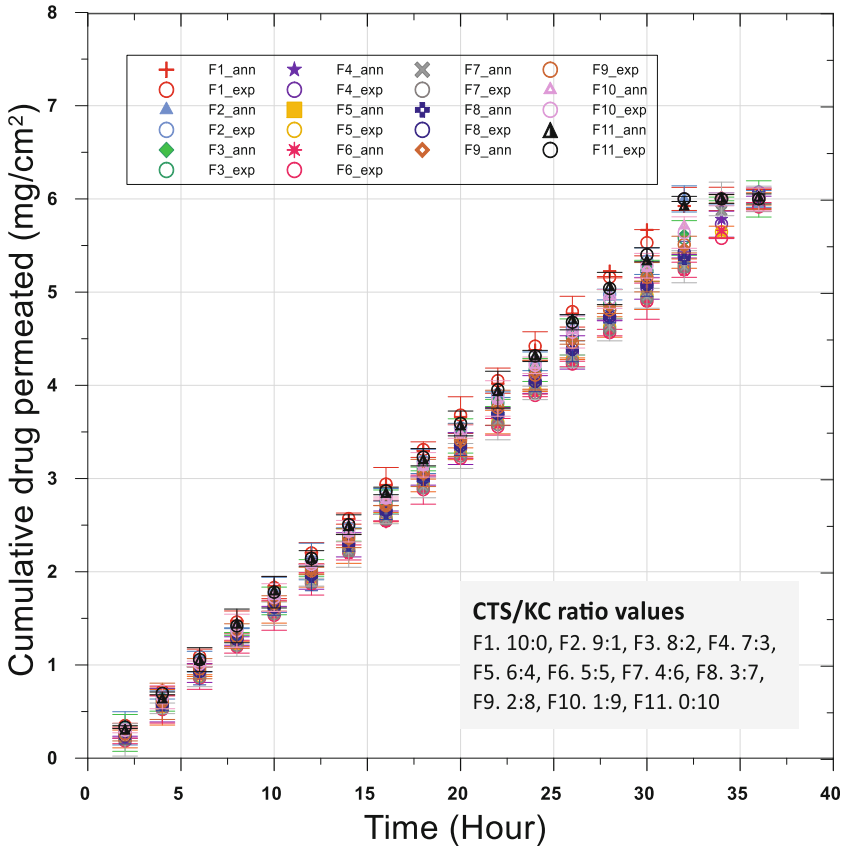

Fig. 9 Experimental and predicted in vitro skin permeation of DS from topical patches

It has been found that the results of DS release kinetics from the set of patches have a similar profile and small differences from changes in the studied formulations have been observed. However, statistical analysis using the one-way ANOVA indicated that there was a significant difference between the formulations with $p < 0.05$. This is probably due to the reproducibility of the formulation factors affecting the in vitro dissolution data to focus only on the evaluation of the effect of the CTS/KC ratio on the release and permeation of the drug. The low value of the SD in the uniformity of the thickness and the drug content (see Table 3) showed that the distribution of the drug in the patch was uniform and that the variability in the different formulations was also negligible. This ensures that the rheological properties of the molding solution are appropriate and ensures homogeneity of the drug by the solvent evaporation technique. These conditions allow

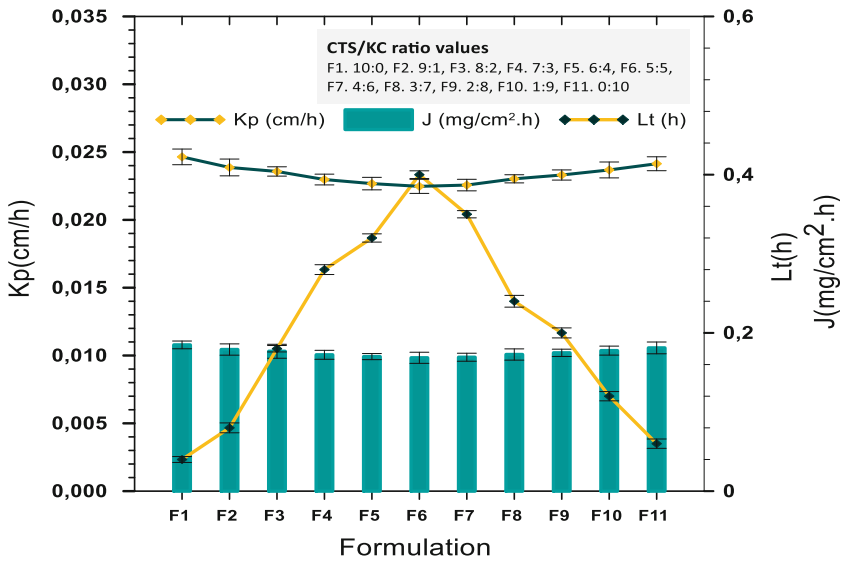

Fig. 10 The permeation parameters of DS topical patches

Table 4 ANN learning results

Inputs	Outputs	Number of hidden layers	Number of neurons in the hidden layer	Number of learning data	Maximum epochs	MSE
• CTS amount • KC amount • Time	• Cumulative drug release (%) • Cumulative drug permeation (mg/cm^2)	01	10	178	650	3.46×10^{-5}

to evaluate the effect of the CTS/KC ratio on drug release and permeation.

The design of the experiment was explored to study the effect of critical variables on the permeation characteristics of cross-linked chitosan membranes, where a central composite design model was applied to simulate the permeation of DS through rat skin [66]. It was proposed that similarly derived mathematical models can be used for the estimation of drug permeation, and the obtained model can be used to design chitosan membranes to simulate the permeation of drugs through different species of animal skin.

ANN modeling result

Most of the experimental data was used to develop the neural network and the training set; the remaining part was left to check the comparison between the number of membership functions assigned to each structure and the RMSE values. MATLAB 7.10.1 software was used to compute, for each unique point of data, the corresponding predicted value accuracy and effectiveness of the ANN model, which is the validation data set. For the optimization of the ANN, the inputs used for the ANN formation were the two independent variables, the polymers ratio (CTS/KG), and the time (t). These variables had a direct effect on the release and diffusion rates of DS, which represented the output variables.

After several tests, a relative error measurement was reached ($MSE = 3.46 \times 10^{-5}$) indicating that the optimal ANN model was obtained. In Table 4, the different parameters of the developed ANN, the structure, and the learning phase results of the trained ANN, using the MATLAB® Neural Network Toolbox (Version 7.10.1), are given. Twenty unique datapoints were kept for the test phase, while another 20 datapoints, from the training set, were used to test and validate the neural model and to validate the synthetized ANN.

Figures 7 and 9 represent the comparison between the simulated ANN and experimental output data (198 sets). The predicted cumulative drug release and permeation efficiency of the ANN results were close to the training and testing data given to the network. The performance of the ANN upon training with the test data was revealed by the trends between the experimental and the neural predicted patterns. The ANN was found to efficiently predict the release and diffusion rates within the range of data contained in the training set.

According to the results given in Table 5, the comparison between a few values calculated by the ANN model and the experimental data showed the excellent performance of this model, which is confirmed by the obtained absolute errors that varied between 0.00 and 3.65 for cumulative release and between 0.00 and 0.08 for the cumulative permeation. Also, the accuracy of the ANN model can be confirmed regarding the prediction of a few sets of data that were not used in the learning step modeling (italic entries in Table 5). This result shows the capability of the established ANN model to predict the drug release profile of each formulation. As for the in vitro skin permeation, the ANN model predicted the permeation of the drug, which can save time and products in experimental tests in upcoming studies.

Modeling validation

The predicted versus experimental values of DS release and permeation for all trial formulations are represented in Fig. 11 to show the ANN model performance. Most of the points were close to the bisector, which revealed a perfect fit between the predicted values and the experimental values. According to this result, the ANN was found to predict the release and the permeation profiles in a significant way, and it simultaneously demonstrated the influence of the formulation parameters on the release and diffusion mechanisms.

Conclusion

In this study, the development of DS skin-delivery systems using biopolymer matrix patches was explored. The prepared formulations were intended to sustain the release rate of DS, with improved bioadhesive properties and reduced toxicity, which ultimately improved their therapeutic efficacy. This investigation revealed that matrices based on CTS/KC provided a favorable device for the development of topical patches with interesting physicochemical, bioadhesive, and mechanical

Table 5 Comparison testing between experimental and predicted values

CTS	KC	Time	Exp. cumulative release (%)	Exp. cumulative permeated (mg/cm^2)	ANN predicted cumulative release	ANN predicted cumulative permeated	Release absolute error	Perm absolute error
10	0	4	22,206	0.720	21,295	0.637	0.91	0.08
10	0	6	31,216	1090	31,143	1069	0.07	0.02
10	0	18	78,553	3310	78,481	3298	0.07	0.01
10	0	22	92,975	4050	93,867	4017	0.89	0.03
10	0	26	100,000	4790	99,994	4770	0.01	0.02
9	1	2	11,112	0.320	11,040	0.295	0.07	0.03
9	1	4	20,309	0.678	20,328	0.610	0.02	0.07
9	1	10	45,072	1752	45,030	1761	0.04	0.01
9	1	14	60,400	2468	60,373	2464	0.03	0.00
9	1	30	100,000	5332	100,000	5435	0.00	0.10
9	1	36	100,000	6000	100,000	6041	0.00	0.04
8	2	4	17,865	0.625	18,085	0.585	0.22	0.04
8	2	6	25,942	0.979	26,236	0.971	0.29	0.01
8	2	8	33,802	1333	33,698	1339	0.10	0.01
8	2	20	78,532	3457	78,408	3462	0.12	0.01
8	2	22	85,729	3811	85,513	3820	0.22	0.01
8	2	28	99,971	4873	99,934	4844	0.04	0.03
7	3	4	14,557	0.569	14,574	0.559	0.02	0.01
7	3	8	28,912	1257	29,114	1281	0.20	0.02
7	3	10	36,060	1601	36,282	1615	0.22	0.01
7	3	30	99,934	5041	99,990	5047	0.06	0.01
7	3	32	99,934	5385	100,000	5425	0.07	0.04
7	3	34	99,934	5729	100,000	5781	0.07	0.05
6	4	4	11,303	0.546	11,098	0.538	0.21	0.01
6	4	10	30,970	1566	30,271	1556	0.70	0.01
6	4	14	44,841	2246	44,496	2213	0.35	0.03
6	4	28	96,119	4626	96,126	4588	0.01	0.04
6	4	30	96,119	4966	99,768	4914	3.65	0.05
5	5	6	14,424	0.859	14,737	0.873	0.31	0.01
5	5	8	20,371	1196	20,498	1209	0.13	0.01
5	5	10	26,626	1533	26,832	1529	0.21	0.00
5	5	12	33,138	1870	33,657	1850	0.52	0.02
5	5	16	46,801	2544	47,987	2522	1.19	0.02
5	5	18	53,906	2881	55,038	2873	1.13	0.01
5	5	20	61,171	3218	61,911	3225	0.74	0.01
5	5	30	99,507	4903	99,484	4884	0.02	0.02
4	6	4	10,686	0.535	10,892	0.545	0.21	0.01
4	6	14	45,134	2227	44,728	2218	0.41	0.01
4	6	16	52,626	2565	52,353	2562	0.27	0.00
4	6	18	60,259	2904	59,830	2914	0.43	0.01
4	6	24	83,889	3919	82,615	3958	1.27	0.04
4	6	32	100,000	5272	99,995	5270	0.01	0.00
3	7	6	20,606	0.930	20,711	0.936	0.11	0.01
3	7	10	35,231	1622	35,582	1621	0.35	0.00
3	7	22	80,626	3698	80,945	3691	0.32	0.01
3	7	24	88,339	4044	88,726	4037	0.39	0.01
3	7	26	96,084	4390	95,610	4382	0.47	0.01

Table 5 (continued)

CTS	KC	Time	Exp. cumulative release (%)	Exp. cumulative permeated (mg/cm^2)	ANN predicted cumulative release	ANN predicted cumulative permeated	Release absolute error	Perm absolute error
3	7	32	100,000	5428	99,998	5359	0.00	0.07
2	8	6	24,109	0.960	23,889	0.975	0.22	0.01
2	8	8	31,869	1310	31,774	1338	0.09	0.03
2	8	10	39,570	1660	39,541	1677	0.03	0.02
2	8	12	47,225	2010	47,289	2010	0.06	0.00
2	8	18	69,981	3060	69,980	3051	0.00	0.01
2	8	20	77,511	3410	77,466	3408	0.04	0.00
2	8	30	99,975	5160	99,989	5162	0.01	0.00
1	9	20	81,245	3503	81,010	3483	0.23	0.02
0	10	2	10,674	0.333	10,453	0.311	0.22	0.02
0	10	14	61,505	2505	61,452	2497	0.05	0.01
0	10	24	99,905	4315	98,222	4327	1.68	0.01
0	10	26	99,905	4677	99,815	4713	0.09	0.04
0	10	36	99,905	6000	99,844	6030	0.06	0.03

properties. The in vitro permeation results indicated that CTS/KC at 1/1 was the best ratio for the sustained release of the drug for a period over 36 h. Finally, it was concluded that optimization of the drug release and drug permeation from topical patches could be widely achieved using an optimum ratio of polymers to greatly extend the usage period, which leads to improvements in the patient's comfort and treatment compliance. Diffusion models were useful to optimize the design of drugs and their formulations from the physicochemical perspective. However, the ANN used to predict the release of DS and its skin permeability from the complex polyelectrolyte matrices, CTS-KC, provided prediction data with reasonable accuracy. The relevant feasibility to use the same ANN model to predict both the diffusion and the dissolution kinetics profiles was successfully realized, and it represented an original alternative to the different traditional release and diffusion modeling.

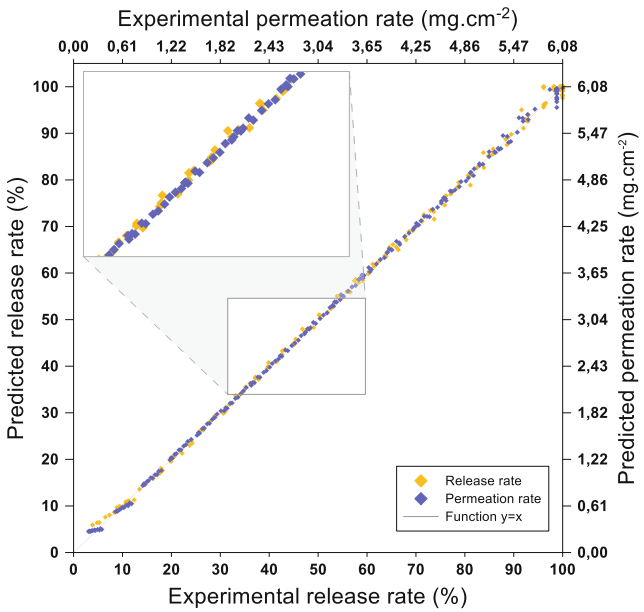

Fig. 11 Point cloud representing the ANN predicted values as a function of the experimental data

Compliance with ethical standards

Conflict of interest The authors declare that they have no conflict of interest.

References

1. Xi H, Cun D, Xiang R, Guan Y, Zhang Y, Li Y, et al. Intra-articular drug delivery from an optimized topical patch containing teriflunomide and lornoxicam for rheumatoid arthritis treatment: does the topical patch really enhance a local treatment? J Control Release. 2013;169(1):73–81.
2. Ita KB. Transdermal drug delivery: progress and challenges. J Drug Deliv Sci Technol 2014;24(3):245–50.
3. Komatsu T, Sakurada T. Comparison of the efficacy and skin permeability of topical NSAID preparations used in Europe. Eur J Pharm Sci. 2012;47(5):890–5.
4. Schoellhammer CM, Blankschtein D, Langer R. Skin permeabilization for transdermal drug delivery: recent advances and future prospects. Expert Opin Drug Deliv 2014;11(3):393–407.
5. Bonsu MA, Ofori-Kwakye K, Kipo SL, Boakye-Gyasi ME, Fosu M-A. Development of oral dissolvable films of diclofenac sodium for osteoarthritis using albizia and khaya gums as hydrophilic film formers. J Drug Deliv 2016;2016:1–11.
6. van den Hoven JM, Van Tomme SR, Metselaar JM, Nuijen B, Beijnen JH, Storm G. Liposomal drug formulations in the treatment of rheumatoid arthritis. Mol Pharm. 2011;8(4):1002–15.

7. Nidhi M, Patro MN, Kusumvalli S, Kusumdevi V Development of transmucosal patch loaded with anesthetic and analgesic for dental procedures and in vivo evaluation, Int J Nanomedicine 2016
8. Escribano E, Calpena AC, Queralt J, Obach R, Doménech J. Assessment of diclofenac permeation with different formulations: anti-inflammatory study of a selected formula. Eur J Pharm Sci. 2003;19(4):203–10.
9. Zhao L, Li Y, Fang L, Ren C, Xu Y, He Z. Effect of O-acylmenthol and salt formation on the skin permeation of diclofenac acid. Drug Dev Ind Pharm. 2009;35(7):814–26.
10. Krishna R, Nataraj M. Efficacy of a single dose of a transdermal diclofenac patch as pre–emptive postoperative analgesia: a comparison with intramuscular diclofenac. South. African J Anaesth Analg 2012;18(4):194–7.
11. Zhang Y, Cun D, Kong X, Fang L. Design and evaluation of a novel transdermal patch containing diclofenac and teriflunomide for rheumatoid arthritis therapy. Asian J Pharm Sci 2014;9(5):251–9.
12. Malviya N. Design and development of a novel transmucosal patch embedded with diclofenac diethylamine loaded solid lipid nanoparticles. J Young Pharm 2015;7(1):45–55.
13. Costa EM, Silva S, Costa MR, Pereira M, Campos DA, Odila J, et al. Chitosan mouthwash: toxicity and in vivo validation. Carbohydr Polym. 2014;111:385–92.
14. Hamman JH. Chitosan based polyelectrolyte complexes as potential carrier materials in drug delivery systems. Mar Drugs 2010;8(4):1305–22.
15. Luo Y, Wang Q. Recent development of chitosan-based polyelectrolyte complexes with natural polysaccharides for drug delivery. Int J Biol Macromol. 2014;64:353–67.
16. Wu Q–X, Lin D–Q, Yao S–J. Design of chitosan and its water soluble derivatives-based drug carriers with polyelectrolyte complexes. Mar Drugs 2014;12(12):6236–53.
17. Volod'ko AV, Davydova VN, Chusovitin E, Sorokina IV, Dolgikh MP, Tolstikova TG, et al. Soluble chitosan–carrageenan polyelectrolyte complexes and their gastroprotective activity. Carbohydr Polym. 2014;101:1087–93.
18. Rebouh S, Bouhedda M, Hanini S, Djellal A. Neural modeling adsorption of copper, chromium, nickel, and lead from aqueous solution by natural wastes. In: Progress in clean energy, Volume 1. Cham: Springer; 2015. p. 341–56.
19. Rebouh S, Lefnaoui S, Bouhedda M, Yahoum MM, Hanini S. Neuro–fuzzy modeling of ibuprofen–sustained release from tablets based on different cellulose derivatives. Drug Deliv Transl Res 2018;9:162–77.
20. Mendyk A, Jachowicz R Decision support systems for pharmaceutical formulation development based on artificial neural networks, Decis Support Syst, 2010.
21. Takayama K, Morva A, Fujikawa M, Hattori Y, Obata Y, Nagai T. Formula optimization of theophylline controlled-release tablet based on artificial neural networks. J Control Release. 2000;68(2):175–86.
22. Barmpalexis P, Kachrimanis K, Georgarakis E. Solid dispersions in the development of a nimodipine floating tablet formulation and optimization by artificial neural networks and genetic programming. Eur J Pharm Biopharm. 2011;77(1):122–31.
23. Takayama K, Fujikawa M, Nagai T. Artificial neural network as a novel method to optimize pharmaceutical formulations. Pharm Res. 1999;16(1):1–6.
24. Ibrić S, Jovanović M, Djurić Z, Parojcić J, Solomun L. The application of generalized regression neural network in the modeling and optimization of aspirin extended release tablets with Eudragit RS PO as matrix substance. J Control Release. 2002;82(2–3):213–22.
25. Ibrić S, Jovanović M, Djurić Z, Parojcić J, Petrović SD, Solomun L, et al. Artificial neural networks in the modeling and optimization of aspirin extended release tablets with Eudragit L 100 as matrix substance. AAPS PharmSciTech. 2003;4(1):E9.
26. Chen Y, McCall TW, Baichwal AR, Meyer MC. The application of an artificial neural network and pharmacokinetic simulations in the design of controlled-release dosage forms. J Control Release. 1999;59(1):33–41.
27. Zupančič Božič D, Vrečer F, Kozjek F. Optimization of diclofenac sodium dissolution from sustained release formulations using an artificial neural network. Eur J Pharm Sci. 1997;5(3):163–9.
28. Hussain AS, Yu X, Johnson RD. Application of neural computing in pharmaceutical product development. Pharm Res. Oct. 1991;8(10):1248–52.
29. Rebouh S, Bouhedda M, Hanini S. Neuro-fuzzy modeling of Cu(II) and Cr(VI) adsorption from aqueous solution by wheat straw. Desalin Water Treat. 2016;57(14):6515–30.
30. Lefnaoui S, Rebouh S, Bouhedda M, Yahoum MM, Hanini S, Artificial neural network modeling of sustained antihypertensive drug delivery using polyelectrolyte complex based on carboxymethyl-kappa-carrageenan and chitosan as prospective carriers, in 2018 International conference on applied smart systems (ICASS), 2018, pp. 1–8.
31. Simon L, Fernandes M. Neural network-based prediction and optimization of estradiol release from ethylene–vinyl acetate membranes. Comput Chem Eng. 2004;28(11):2407–19.
32. Lefnaoui S, Moulai-Mostefa N, Yahoum MM, Gasmi SN. Design of antihistaminic transdermal films based on alginate–chitosan polyelectrolyte complexes: characterization and permeation studies. Drug Dev Ind Pharm. 2018;44(3):432–43.
33. Kriplani P. Formulation and evaluation of transdermal patch of diclofenac sodium. Glob. J. Pharm. Pharm. Sci. 2018;4(5).
34. Nasir F, Iqbal Z, Khan JA, Khan A, Khuda F, Ahmad L, et al. Development and evaluation of diclofenac sodium thermorevesible subcutaneous drug delivery system. Int J Pharm. 2012;439(1–2):120–6.
35. Satheeshababu BK, Shruthinag R. Synthesis and charactersiation of chitosan conjugate; design and evaluation of membrane moderated type transdermal drug delivery system. Indian J Pharm Sci. 2015;77(4):405–12.
36. Vermani K, Garg S, Zaneveld LJD. Assemblies for in vitro measurement of bioadhesive strength and retention characteristics in simulated vaginal environment. Drug Dev Ind Pharm. 2002;28(9):1133–46.
37. Patel VM, Prajapati BG, Patel MM. Design and characterization of chitosan-containing mucoadhesive buccal patches of propranolol hydrochloride. Acta Pharma. 2007;57(1):61–72.
38. Singhvi G, Singh M. Review: in vitro drug release characterization models. Int J Pharm Stud Res. 2011;2:77–84.
39. Güngör S, Erdal M, Özsoy Y, Plasticizers in transdermal drug delivery systems, in Recent advances in plasticizers, 2012.
40. Xu P-G, Lei X-F, Ren B-D, Lv S-Y, Zhang J-L. Diclofenac transdermal patch versus the sustained release tablet: a randomized clinical trial in rheumatoid arthritic patients. Trop J Pharm Res. 2017;16(2):477–482–482.
41. Kenawi IM, Barsoum BN, Youssef MA. Cetirizine dihydrochloride interaction with some diclofenac complexes. Eur J Pharm Sci. 2005;26(3–4):341–8.
42. Kozakevych RB, Bolbukh YM, Tertykh VA. Controlled release of diclofenac sodium from silica–chitosan composites. World J Nano Sci Eng. 2013;03:69–78.
43. U. S. P. Convention, U.S. Pharmacopeia National Formulary 2016: USP 39 NF 34, Supplement edition. Rockville, Md.: United States Pharmacopeial, 2016.
44. Can A, Erdal M, Güngör S, Özsoy Y. Optimization and characterization of chitosan films for transdermal delivery of ondansetron. Molecules. 2013;18(5):5455–71.
45. Srinivasa PC, Ramesh MN, Tharanathan RN. Effect of plasticizers and fatty acids on mechanical and permeability characteristics of chitosan films. Food Hydrocoll. 2007;21(7):1113–22.

46. Cerqueira MA, Souza BWS, Teixeira JA, Vicente AA. Effects of interactions between the constituents of chitosan-edible films on their physical properties. Food Bioprocess Technol. 2012;5(8): 3181–92.
47. Casariego A, Souza BWS, Cerqueira MA, Teixeira JA, Cruz L, Díaz R, et al. Chitosan/clay films' properties as affected by biopolymer and clay micro/nanoparticles' concentrations. Food Hydrocoll. 2009;23(7):1895–902.
48. Xu YX, Kim KM, Hanna MA, Nag D. Chitosan–starch composite film: preparation and characterization. Ind Crop Prod. 2005;21(2): 185–92.
49. Siyawamwaya M, Choonara YE, Bijukumar D, Kumar P, Toit LCD, Pillay V. A review: overview of novel polyelectrolyte complexes as prospective drug bioavailability enhancers. Int J Polym Mater Polym Biomater. 2015;64(18):955–68.
50. Lal N, Dubey J, Gaur P, Verma N, Verma A. Chitosan based in situ forming polyelectrolyte complexes: a potential sustained drug delivery polymeric carrier for high dose drugs. Mater Sci Eng C Mater Biol Appl. 2017;79:491–8.
51. Mazumder MAJ. Polyelectrolyte complexation between cationic and anionic polyelectrolytes with complementary polymer-bound reactive groups of amine and acetoacetate: effect of mono- and divalent salts. Iran Polym J. 2014;23(6):445–55.
52. van der Gucht J, Spruijt E, Lemmers M, Cohen Stuart MA. Polyelectrolyte complexes: bulk phases and colloidal systems. J Colloid Interface Sci. Sep. 2011;361(2):407–22.
53. Dubey J, Verma A, Verma N. Evaluation of chitosan based polymeric matrices for sustained stomach specific delivery of propranolol hydrochloride. Indian J Mater Sci. 2015;2015:1–9.
54. Sakiyama T, Chu C-H, Fujii T, Yano T. Preparation of a polyelectrolyte complex gel from chitosan and κ-carrageenan and its pH-sensitive swelling. J Appl Polym Sci. 1993;50(11):2021–5.
55. Sakiyama T, Takata H, Kikuchi M, Nakanishi K. Polyelectrolyte complex gel with high pH-sensitivity prepared from dextran sulfate and chitosan. J Appl Polym Sci. 1999;73(11):2227–33.
56. Hugerth A, Caram-Lelham N, Sundelöf L-O. The effect of charge density and conformation on the polyelectrolyte complex formation between carrageenan and chitosan. Carbohydr Polym. 1997;34(3): 149–56.
57. Ghosal K, Chandra A, Rajabalaya R, Chakraborty S, Nanda A. Mathematical modeling of drug release profiles for modified hydrophobic HPMC based gels. Pharmazie. 2012;67(2):147–55.
58. Mishra D, Khare P, Shanker K, Singh DK, Luqman S. Controlled delivery systems of cellulose matrix for oxytetracycline: in vitro dissolution. Eur J Mol Clin Med. 2016;3(2):66–72.
59. Dash S, Murthy PN, Nath L, Chowdhury P. Kinetic modeling on drug release from controlled drug delivery systems. Acta Pol Pharm. 2010;67(3):217–23.
60. Jung EC, Maibach HI. Animal models for percutaneous absorption. J Appl Toxicol. 2015;35(1):1–10.
61. Abd E, Yousuf S, Pastore M, Telaprolu K, Mohammed Y, Namjoshi S, et al. Skin models for the testing of transdermal drugs. CPAA. 2016;8:163–76.
62. Todo H. Transdermal permeation of drugs in various animal species. Pharmaceutics. 2017;9(3).
63. Takeuchi H, et al. Usefulness of rat skin as a substitute for human skin in the in vitro skin permeation study. Exp Anim. 2011;60(4): 373–84.
64. Yeole PG, Galgatte UC, Babla IB, Nakhat PD, Design and evaluation of xanthan gum-based sustained release matrix tablets of diclofenac sodium, Indian J Pharm Sci, vol. 68, no. 2, 2006.
65. Argin-Soysal S, Kofinas P, Lo YM. Effect of complexation conditions on xanthan–chitosan polyelectrolyte complex gels. Food Hydrocoll. 23(1):202–9.
66. Dureja H, Tiwary AK, Gupta S. Simulation of skin permeability in chitosan membranes. Int J Pharm. 2001;213(1–2):193–8.